

## APPLIED PHYSICS

# Direct imaging of an inhomogeneous electric current distribution using the trajectory of magnetic half-skyrmions

Senfu Zhang<sup>1</sup>, Xichao Zhang<sup>2</sup>, Junwei Zhang<sup>1,3</sup>, Arnab Ganguly<sup>1</sup>, Jing Xia<sup>2</sup>, Yan Wen<sup>1</sup>, Qiang Zhang<sup>1</sup>, Guoqiang Yu<sup>4</sup>, Zhipeng Hou<sup>5</sup>, Wenhong Wang<sup>4</sup>, Yong Peng<sup>3</sup>, Gang Xiao<sup>6</sup>, Aurelien Manchon<sup>1</sup>, Jürgen Kosel<sup>7</sup>, Yan Zhou<sup>2</sup>, Xi-Xiang Zhang<sup>1\*</sup>

The direct imaging of current density vector distributions in thin films has remained a daring challenge. Here, we report that an inhomogeneous current distribution can be mapped directly by the trajectories of magnetic half-skyrmions driven by an electrical current in Pt/Co/Ta trilayer, using polar magneto-optical Kerr microscopy. The half-skyrmion carries a topological charge of 0.5 due to the presence of Dzyaloshinskii-Moriya interaction, which leads to the half-skyrmion Hall effect. The Hall angle of half-skyrmions is independent of current density and can be reduced to as small as 4° by tuning the thickness of the Co layer. The Hall angle is so small that the elongation path of half-skyrmion approximately delineates the invisible current flow as demonstrated in both a continuous film and a curved track. Our work provides a practical technique to directly map inhomogeneous current distribution even in complex geometries for both fundamental research and industrial applications.

## INTRODUCTION

The accurate determination of the electric current distribution in a conductor, including its magnitude and direction, is extremely essential for designing micro/nanodevices and integrated circuits, particularly in the case of an inhomogeneous distribution due to geometric constraint. Over the years, various techniques, such as scanning superconducting quantum interference device (SQUID) probe (1–6), scanning Hall probe (7, 8), and scanning tunneling magnetoresistance probes (9, 10), have been developed to map the current density distributions. These techniques probe the magnetic stray field generated by the current and then reconstruct the current density distribution based on the Biot-Savart law (1–10). These approaches do not provide a direct observation of the current, and the complex relation between the local stray field vector and the current density vector hampers the accurate mapping of the current density and direction (1–10). Moreover, these techniques are costly specialized instruments developed for the industry. Some scanning probes also need extreme conditions, such as very low temperatures, for example, in the case of SQUID probes. The current distribution that includes both the density and the direction can, in principle, be numerically simulated using finite element calculation (11, 12). However, because of the oversimplified model and difficulties to take into account the nonuniformity or tiny cracks in the real conductor, the results may not be convincing and trustable. To this day, it is still experimentally impossible to directly observe and map the in-

homogeneous current distribution. Here, we demonstrate that magneto-optical Kerr effect (MOKE) microscopy commonly found in most magnetic materials laboratories can be used to directly map the inhomogeneous current density distribution vector (or distribution of electric field lines) in thin films. The key mechanism involved in the process is the motion of magnetic half-skyrmions (13) driven by an electrical current in heavy metal/ferromagnetic metal/heavy metal trilayers.

When an in-plane current flows in a heavy metal/ferromagnetic metal heterostructure, a spin current is generated within the heavy metal layer and is injected into the ferromagnetic layer because of the spin Hall effect (SHE) (14–20). The orientation of the spins  $\mathbf{p}$  injected into the ferromagnetic layer is determined by

$$\mathbf{p} = -\text{sgn} \theta_{\text{SH}} (\mathbf{z} \times \mathbf{j}) \quad (1)$$

where  $\theta_{\text{SH}}$  is the spin Hall angle of the heavy metal and  $\mathbf{z}$  and  $\mathbf{j}$  are the unit vectors of the interface normal and the electrical current density, respectively (16, 17, 20). If the polarization of injected spins is not parallel to the magnetization in the ferromagnetic layer, then this misalignment will generate spin torques that, in turn, through their accumulated actions, will induce the magnetization direction of the ferromagnetic layer to be switched, or bring the domain walls into motion (15–18, 20–22), when the current density is large enough. Recent studies have reported the observation of a current-driven motion of skyrmions in a heavy metal/ferromagnetic metal heterostructure due to the SHE (21–23). The paths of the skyrmions are governed by the skyrmion Hall effect (22). In principle, if the Hall angle is a known entity, then the current direction can be extracted from the trajectories of the skyrmions. However, the experimental results show that the skyrmion Hall angle depends notably on the current density due to the presence of disorder (22–24) and that a large number of images have to be taken during the application of current to record the paths of the skyrmions (21–23). This procedure is not an effective way of recording the moving paths. Moreover, it requires the application of an external magnetic field to stabilize the isolated skyrmions (14, 21, 22, 25–32).

<sup>1</sup>Physical Science and Engineering Division (PSE), King Abdullah University of Science and Technology (KAUST), Thuwal 23955-6900, Saudi Arabia. <sup>2</sup>School of Science and Engineering, The Chinese University of Hong Kong, Shenzhen, Guangdong 518172, China. <sup>3</sup>Key Laboratory for Magnetism and Magnetic Materials of the Ministry of Education, Lanzhou University, Lanzhou 730000, China. <sup>4</sup>State Key Laboratory of Magnetism, Institute of Physics, Chinese Academy of Sciences, Beijing 100190, China. <sup>5</sup>Guangdong Provincial Key Laboratory of Quantum Engineering and Quantum Materials and Institute for Advanced Materials, South China Academy of Advanced Optoelectronics, South China Normal University, Guangzhou 510006, China. <sup>6</sup>Department of Physics, Brown University, Providence, RI 02912, USA. <sup>7</sup>Computer, Electrical and Mathematical Sciences and Engineering Division, KAUST, Thuwal 23955-6900, Saudi Arabia.

\*Corresponding author. Email: xixiang.zhang@kaust.edu.sa

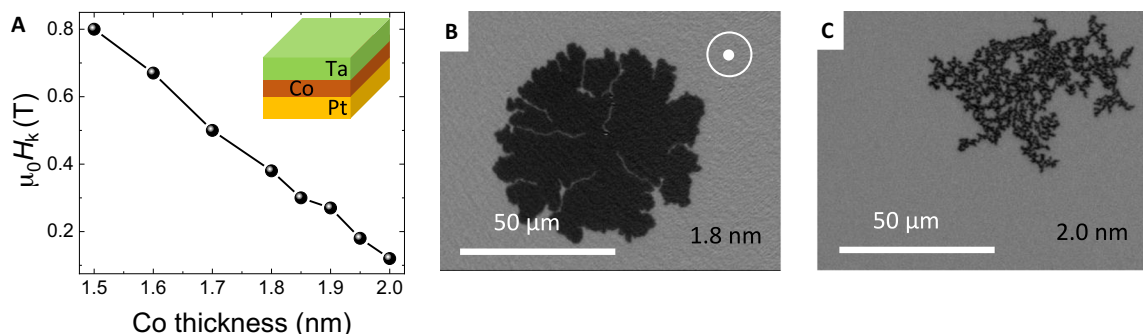


**Fig. 1. Magnetic properties and domain images.** (A) Effective perpendicular anisotropy field  $\mu_0 H_k$  as a function of the thickness of the Co layer. Inset shows the schematic structure of Pt (3 nm)/Co ( $t$ )/Ta (2 nm), with  $t$  ranging from 1.5 to 2.0 nm. (B and C) MOKE microscopy image of a typical domain structure created in the films, with (B)  $t = 1.8$  nm and (C)  $t = 2.0$  nm. The black areas represent the magnetic domain, with a negative magnetization ( $M_z < 0$ ) created by the application of a negative field to positively saturated films with  $M_z > 0$  (white area).

In our study, we observe the growth of very narrow strip domains driven by electric current pulses, in Pt/Co/Ta films, at zero magnetic field. The growth of these strip domains can be ascribed to the current-driven motion of the half-skyrmions (13). We find that the Hall angle of the half-skyrmions is independent of the current density. Therefore, it is easy to extract the current direction from the images of the domain patterns generated by the electrical current, particularly in the case of an inhomogeneous current density. Our ability to reduce the Hall angle to a small value (as small as  $4^\circ$ ) by carefully tuning the effective perpendicular magnetic anisotropy (PMA) (obtained by varying the thickness of the Co layer) allows us to directly map the current distribution using the moving paths of the half-skyrmions.

## RESULTS

### Magnetic characterization of the samples

We deposit Ta (5 nm)/Pt (3 nm)/Co ( $t$ )/Ta (2 nm) films with different thicknesses of the Co layer (see Materials and Methods). Hysteresis loops (see fig. S1) indicate that all samples have PMA. However, the effective anisotropy field  $\mu_0 H_k$  decreases as the thickness of Co layer increases, as shown in Fig. 1A. To fully understand the magnetization reversal behaviors of these samples, we observe their magnetic domain structures using a polar MOKE microscope (see section S1). Figure 1 (B and C) shows two typical magnetic domain patterns, captured after a few field pulses, for samples with thickness  $t = 1.8$  or 2.0 nm. The dendritic growth of downward domains, clearly seen on the images in fig. S2, may be ascribed to the existence of Dzyaloshinskii-Moriya interaction (DMI) (21, 30, 31) (see fig. S3) in the sample and the relatively weaker PMA (33, 34). It is obvious that the width of each downward domain decreases as the Co thickness increases (Fig. 1, B and C) because of the decrease of the PMA with increasing  $t$  (Fig. 1A) (33). Note that the density of the effective nucleation sites in our films is very low because of the high homogeneity of the film. Hence, finding a nucleation site sometimes takes a very long time. When  $t$  is larger than 2.0 nm, the PMA of the samples becomes very weak, and the domain sizes are too small to be distinguished using a MOKE microscope. Eventually, the magnetization will lie in the plane of the film, as the PMA further decreases.

### Current-induced half-skyrmion Hall effect

To investigate the current-induced dynamics of the magnetic domain structures, we patterned the film into a long strip track with two elec-

trodes on both long ends, as shown in Fig. 2A. First, labyrinth-like domain patterns are generated (see Materials and Methods) in an upward saturated sample with  $t = 1.95$  nm, as shown in Fig. 2B. Current pulses with a density  $j = 5.2 \times 10^{10}$  A m $^{-2}$  are then applied to the strip track, for a total duration  $\tau = 0.1$  s, along the  $+x$  direction where the current density is normalized by the total thickness of Ta (5 nm)/Pt (3 nm)/Co (1.95 nm)/Ta (2 nm). Figure 2C shows the Kerr image of the magnetic domain pattern after two current pulses. In this figure, we can clearly see the formation of new parallel, narrow, straight-strip domains with  $M_z < 0$  that grow from the existing labyrinth-like domains. The growing direction of the narrow domains has an almost fixed angle between the current directions ( $+x$ ). Because of the well-defined chirality of the spin textures of the domain walls resulting from the DMI, the front ends of the strip domains can be considered as half-skyrmions with topology number of  $Q = 1/2$ , as shown in the right panel of Fig. 2C (13). Therefore, we may call this phenomenon a “half-skyrmion Hall effect,” with an estimated Hall angle (between the current and elongation directions of the domains in the image) of  $\sim 38^\circ$ . Although the observed phenomenon is slightly different from the current-induced skyrmion Hall effect, where skyrmions move as rigid objects without changing in size, the physics behind both phenomena may still be similar or almost similar. To confirm this, we investigate the relationship between the current directions and the half-skyrmion moving directions. In total, four configurations are studied by varying the directions of magnetization (up and down) and that of the current ( $+x$  and  $-x$ ) (see fig. S6). Figure 2 (D and E) shows the magnetic domain patterns, before and after the application of two current pulses along the  $+x$  direction, with the same current density and duration as used in Fig. 2C in the same sample with a negative saturated magnetization. It is evident that, by reversing the magnetization direction, the moving direction of the half-skyrmions is also reversed because of the opposite topological charge (see the right panel of Fig. 2E) (22). We conclude that the longitudinal component (along the  $x$  direction) of the velocity of the half-skyrmions always follows the direction of the current, i.e., against the direction of the electron flow. This behavior is very similar to that of Néel-type skyrmions in Pt-based trilayer films, where Pt is the bottom layer (21, 23). Moreover, the absolute values of the Hall angles are almost identical for all four configurations.

A model based on Thiele approach (35) has been used to analyze the motion of the half-skyrmions driven by the spin-orbit torque (SOT)

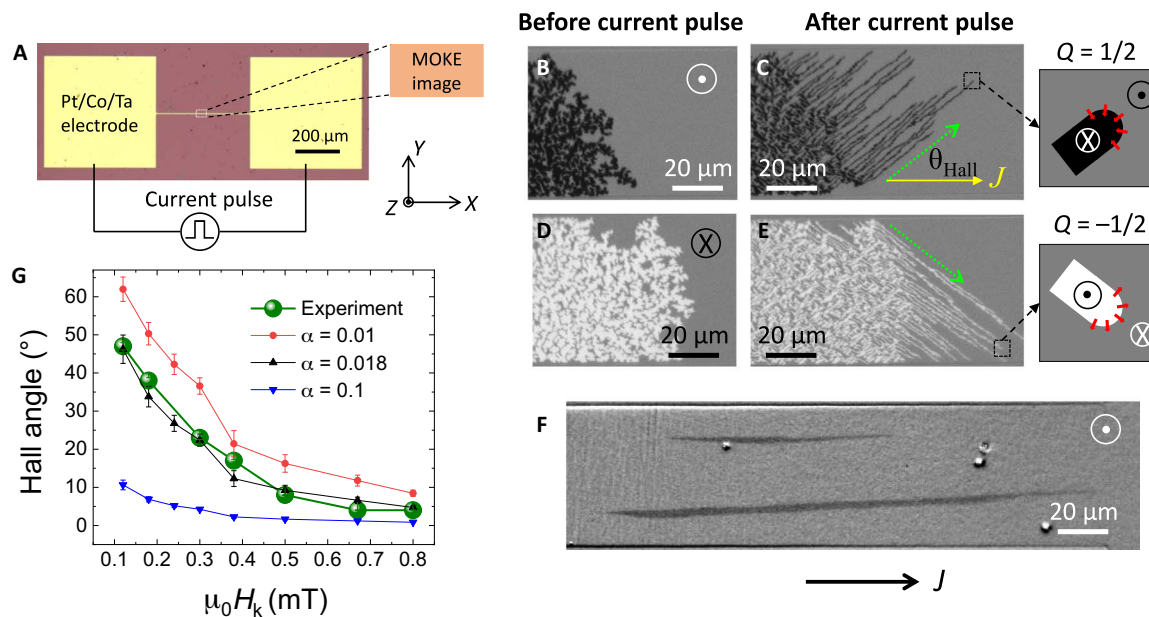


**Fig. 2. Half-skyrmion Hall effect.** (A) Optical microscope image of the long strip track. The electrodes are at both long ends. The width of the track ranges from 30 to 100  $\mu\text{m}$ . (B) MOKE microscopy image of the magnetic domain generated by carefully applying a few negative magnetic field pulses to a positively saturated sample with  $t = 1.95$  nm. The domain nucleated at a random position and grew into the track. (C) Magnetic domain patterns after two current pulses with  $j = 5.2 \times 10^{10}$   $\text{A m}^{-2}$  and  $\tau = 0.1$  s. The yellow arrow indicates the current direction; the green dashed arrow indicates the growth direction of the strip domains. The right panel shows the schematic spin texture of one front end of the strip domains, which is a half-skyrmion with  $Q = 1/2$ . MOKE microscopy image of the (D) magnetic domain patterns with opposite magnetization and (E) after the same two current pulses. (F) The magnetic domain patterns (the path of the half-skyrmions) after 50 current pulses with  $j = 7.64 \times 10^{10}$   $\text{A m}^{-2}$  and  $\tau = 0.1$  s for the sample with  $t = 1.5$  nm. (G) Hall angles of the half-skyrmions as functions of the effective perpendicular anisotropy field  $\mu_0 H_k$ . Large green solid circles: Experimental data. Red dots and triangles are the data calculated on the basis of our theoretical model (Eq. 2), with  $\alpha = 0.01, 0.018$ , and  $0.1$ .

induced by the SHE (see section S2) and to obtain that the Hall angle  $\theta$  of a half-skyrmion is governed by

$$\theta = \arctan \frac{16Q\sqrt{A/K_{\text{eff}}}}{\pi^2\alpha d} \quad (2)$$

where  $Q = 1/2$  is the skyrmion number,  $A$  is the exchange constant,  $K_{\text{eff}}$  is the effective PMA,  $d$  is the half-skyrmion size, and  $\alpha$  is the Gilbert damping constant. According to the above prediction, we investigate the dependence of the Hall angles of the half-skyrmions on the  $K_{\text{eff}}$  by changing the thickness  $t$  of the Co layer, from 1.5 to 2 nm, in a systematic fashion (see fig. S7 and movies S1 and S2). Results are summarized in Fig. 2G with a green solid circle. We find that the Hall angle of the half-skyrmions decreases monotonically, as the effective anisotropy field  $H_k$  increases, without indication of saturation in the low  $H_k$  regime. It is evident that the Hall angle of the half-skyrmions can be much larger in films with an even weaker PMA. However, we find that the magnetic domains in samples with a weaker PMA are too narrow to be distinguished by our MOKE system because of its resolution limits. Another very important piece of information presented in Fig. 2G is that the Hall angle can be reduced down to  $\sim 4^\circ$  by increasing the effective PMA, which is critical to directly map the current flow in thin films, as discussed below.

Using the data shown in fig. S8, the dependence of  $K_{\text{eff}}$  and the size of the half-skyrmion (or width of the strip domain) on the perpendicular anisotropy field ( $\mu_0 H_k$ ) and assuming that  $A = 1 \times 10^{-11}$   $\text{J m}^{-1}$ , we calculate the Hall angles of the half-skyrmions as a function of  $\mu_0 H_k$  using Eq. 2, for  $\alpha = 0.01, 0.018$ , and  $0.1$ . We plot the results together

with the experimental data (Fig. 2G). Experimental data appear to be well described by Eq. 2 with  $\alpha = 0.018$ .

### Current density dependence of the half-skyrmion Hall angle

Current density is also an important parameter for applications, and Eq. 2 predicts that the Hall angle of a half-skyrmion is independent of the driving current. To confirm this prediction experimentally, we vary the current density,  $j$ , applied to a sample with  $t = 1.95$  nm, from  $0 \times 10^{10}$  to  $6.54 \times 10^{10}$   $\text{A m}^{-2}$ ; we also vary the duration of the applied current,  $\tau$ , from 1 ms to 10 s. Results are presented in Fig. 3 (A to D). In these figures, we can clearly see that, even for  $\tau = 10$  s (a nearly constant current), there is a current threshold,  $j_{\text{th}} = 3.76 \times 10^{10}$   $\text{A m}^{-2}$ , to bring the half-skyrmions into motion and consequently trigger the growth of the strip domains (Fig. 3A). With a smaller  $\tau$  and  $j < j_{\text{th}}$ , we do not observe any response of the domain structure to the applied current. For  $j \geq j_{\text{th}}$ , the speed of the half-skyrmions (calculated using the fastest half-skyrmion) increases very slowly, from 1.14 to 68  $\mu\text{m s}^{-1}$ , as  $j$  is increased from  $3.76 \times 10^{10}$  to  $5.2 \times 10^{10}$   $\text{A m}^{-2}$ . When  $j$  becomes larger than  $5.2 \times 10^{10}$   $\text{A m}^{-2}$ , the speed increases sharply, as shown in Fig. 3E. However, even the maximum speed, at  $j = 6.1 \times 10^{10}$   $\text{A m}^{-2}$ , is only 5  $\text{mm s}^{-1}$ , being in the creep-motion regime (36). The Hall angles under different current densities are estimated and summarized in Fig. 3E. We find that the Hall angle is almost independent of the current density and that they remain constant, at a value of approximately  $38^\circ$ , which confirms the above prediction.

### Reconstruction of the inhomogeneous electric current distribution

Because the Hall angle of the half-skyrmions is independent of the applied current density and the trajectories of the half-skyrmions are

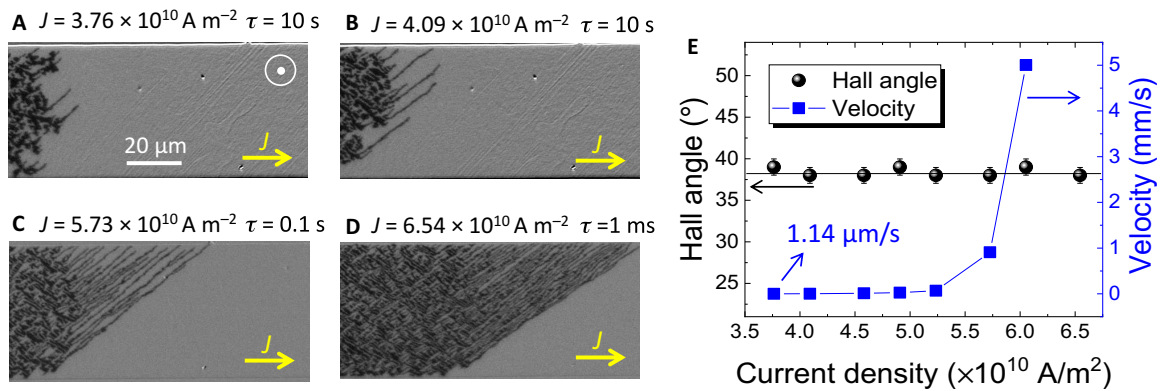


**Fig. 3. Relationship between the half-skyrmion Hall angle and current density.** (A to D) Magnetic domain patterns after application of one current pulse with different  $j$  and  $\tau$ . The yellow arrow indicates the current direction. (E) Dependence of the maximum velocity of the half-skyrmion and the corresponding Hall angles as functions of  $j$ .

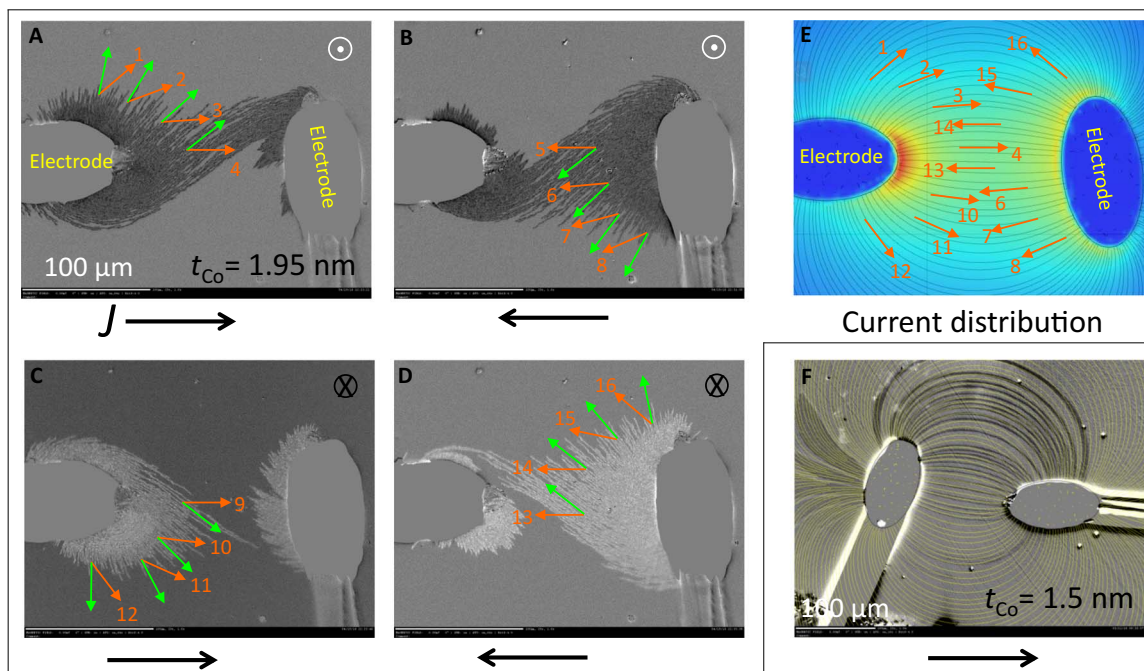


**Fig. 4. Reconstruction of the electric current streamline distribution.** (A to D) Magnetic strip domain patterns after applying a 9-V voltage pulse with  $\tau = 10 \text{ ms}$  on a saturated sample of  $t = 1.95 \text{ nm}$  with a half-skyrmion Hall angle of  $38^\circ$  for four cases with different saturation directions and current directions. The directions of the moving half-skyrmions at four random positions are marked with green arrows. Then, we rotate the arrows about  $+38^\circ$  or  $-38^\circ$  according to the Hall angle to obtain the current directions (orange arrows) at those corresponding locations. (E) Simulated electric current streamline in a pure metallic film with the same configuration as that in (A) to (D). The orange arrows indicate current directions obtained experimentally in (A) to (D). (F) Magnetic strip domain patterns after applying a 9-V voltage pulse with  $\tau = 10 \text{ ms}$  on a saturated sample of  $t = 1.5 \text{ nm}$  with a half-skyrmion Hall angle of  $4^\circ$ . The yellow line represents the simulated electric current streamline in a pure metallic film with the same configuration. Because the electrodes were bonded randomly on the film, the positions of electrodes in (F) are different from that in (A) to (E).

perfectly recorded/reflected by the elongation of the very narrow strip domains, the images of the narrow domains can be used to reconstruct the distribution of the inhomogeneous electric current. To demonstrate the feasibility of this technique, we bond the copper electrode directly on a multilayer film, with  $t = 1.95 \text{ nm}$ , as shown in Fig. 4. We measure the resistance between the two electrodes and find it to be 64.43 ohms. The sample is first magnetized to saturation using a positive magnetic field. When a +9-V voltage pulse with  $\tau = 10 \text{ ms}$  is applied between the two electrodes, a very interesting, well-shaped pattern can be observed on the Kerr image. This shows

that many strip domains are generated near the two electrodes, in areas with the highest current density. Subsequently, the strip domains grow from the left electrode to the right electrode, following a path that is governed by the half-skyrmion Hall effect as shown in Fig. 4A. In this figure, the directions in which the strip domains grow (or the moving direction of the half-skyrmions) are shown at four random positions using green arrows. Considering that the Hall angle is  $38^\circ$  for the sample represented in Fig. 3E, we are able to obtain the current directions (orange arrows) at those four random positions by rotating the green arrow  $38^\circ$  clockwise. When the polarity of the voltage (or current flow

direction) is reversed, the strip domains grow from the right electrode to the left electrode (Fig. 4B). We then saturate the sample with a negative magnetic field, which leads to the creation of upward strip domains that grow from the positive electrode to the negative one with Hall angles opposite to that observed in Fig. 4, A and B, as shown in Fig. 4, C and D. The direction of the strip domain growth and the corresponding direction of electric current at four random positions are also indicated in Fig. 4 (B to D). To verify the validity of the current distribution constructed on the basis of the Kerr images, we calculate the corresponding current distribution using finite element modeling as shown in Fig. 4E (see Materials and Methods). We find that the experimental results reconstructed from the Kerr images match the numerical results very well.

### Direct imaging of the inhomogeneous electric current distribution

As shown in Fig. 2G, the Hall angle decreases sharply as the effective PMA increases and the Hall angle can be reduced down to  $4^\circ$  for the sample with  $t = 1.5$  nm. It is obvious that the strip domain grows almost in alignment with the current direction in the samples. Therefore, the Kerr images of the domain patterns can be considered as a viable direct

mapping technique of an inhomogeneous current distribution. We then perform the same experiment using the  $t = 1.5$  nm sample. Kerr images of the domains obtained with  $V = 9$  V and  $\tau = 10$  ms are shown in Fig. 4F. It is clear that the magnetic domain pattern is very similar to the distribution of the simulated electric current distribution results (yellow line), as shown in Fig. 4F.

In addition, we pattern the film with  $t = 1.5$  nm into a curved track and investigate the trajectory of half-skyrmions driven by current pulses. Figure 5A shows the initial magnetic domain state generated by applying a few negative magnetic field pulses to the positively saturated curved track. Some half-skyrmions are then created from the left entrance of the curved structure when a current pulse with  $j = 7.83 \times 10^{10}$  A m<sup>-2</sup> is applied from left to right. It can be seen that a half-skyrmion with  $Q = 1/2$ , indicated by the yellow dashed circle, moves along the curved conduction path, as shown in Fig. 5 (B to D) (see the detailed process in movie S3). Note that, because the initial state is a wide domain wall (Fig. 5A), the width of the created strip domain at the rear part is also large and that a pinning site, as indicated by the red arrow in Fig. 5C, splits the strip domain and creates one more half-skyrmion, as indicated by the cyan dashed circle. Figure 5E shows that a half-skyrmion with  $Q = -1/2$ , indicated by the red dashed

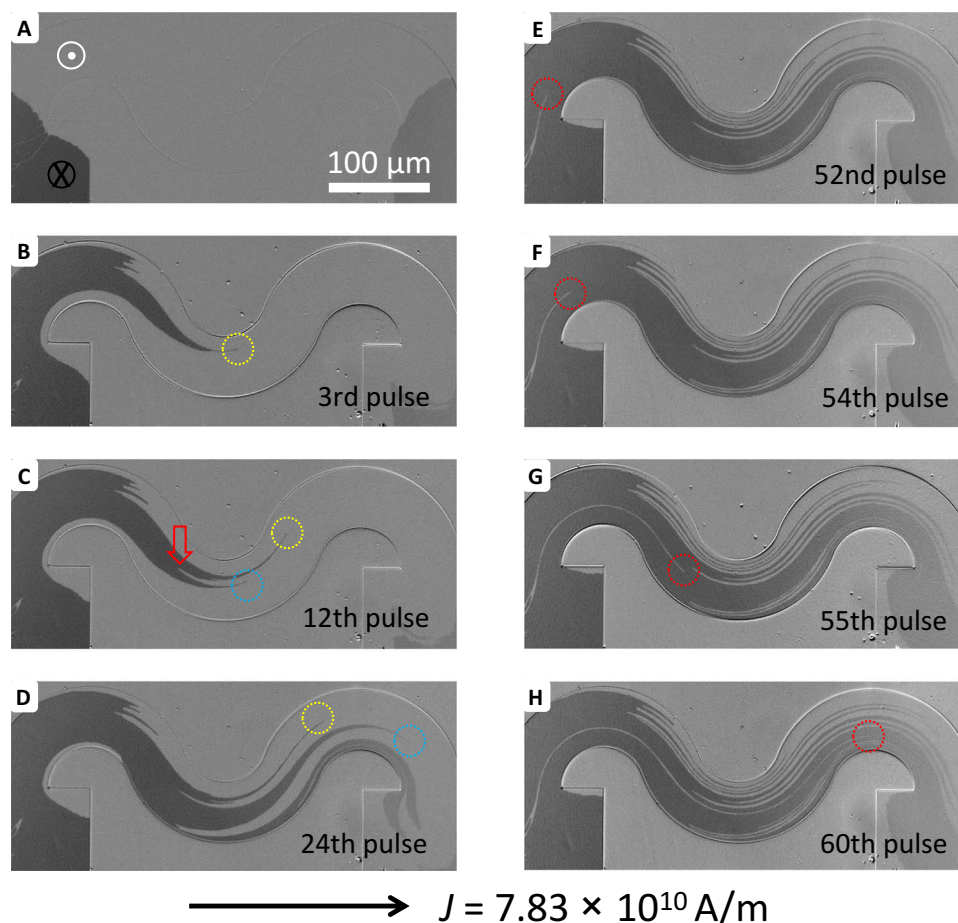


**Fig. 5. Trajectory of half-skyrmions in a curved structure.** (A) MOKE microscopy image of the initial magnetic domain generated by carefully applying a few negative magnetic field pulses to a positively saturated curved structure sample with  $t = 1.5$  nm. (B to H) Magnetic domain patterns after the (B) 3rd, (C) 12th, (D) 24th, (E) 52nd, (F) 54th, (G) 55th, and (H) 60th current pulse with  $j = 7.83 \times 10^{10}$  A m<sup>-2</sup> from left to right. The pulse duration is  $\tau = 0.1$  s before the 39th current pulse and increases to  $\tau = 0.5$  s from the 39th current pulse. The yellow and cyan dashed circles in (B) to (D) indicate the positions of half-skyrmions with  $Q = 1/2$ . The red arrow in (C) indicates a pinning site. The red dashed circles in (E) to (H) indicate the position of a half-skyrmion with  $Q = -1/2$ .

circle, moves into the left side of the curved track. Then, a very beautiful strip domain with uniform width created by the trajectory of the half-skyrmion along the curved track is observed, as shown in Fig. 5 (E to H).

These results demonstrate that the half-skyrmion paths can be used to directly map an inhomogeneous current distribution. For practical applications, to map the current distribution arising from a complex set of the electrodes, one can deposit a heterostructure as simple as Pt/Co/Ta and image the domain pattern using a Kerr microscope. These microscopes are commonly available in most magnetic materials laboratories.

## DISCUSSION

One of the most important features in our observation is that the moving direction of the half-skyrmion does not depend on the current density, which is in stark contrast to the fact that the Hall angle of an individual moving skyrmion depends nearly linearly on the current density in the low-current density regime and saturates at a threshold current density, as observed in a Ta/CoFeB/TaO<sub>x</sub> system by Jiang *et al.* (22). This can be understood as follows.

For an individual skyrmion, its motion can be described by Newton's law, where the skyrmion is considered as a rigid particle and its internal structure and energy are constant. The forces include the effective driving force induced by the current that has a fixed direction (includes both the SOT-induced force and the Magnus force), the pinning force of defects, and the scattering by defects in the materials (37, 38). Under a small current density, the driving force may just be slightly stronger than the pinning force. After each de-pinning process, the kinetic energy (or velocity) of the skyrmion would be quite small. It can then be scattered easily by the random potentials originated from defects again and again, which leads to a random change in velocity (direction and magnitude), most likely, similar to the scattering of electrons by the defects in a conductor. Therefore, the motion of individual skyrmions should be pretty random. By increasing the current density, the driving force will gradually dominate over other forces; consequently, the motion of individual skyrmions will also be gradually governed by the driving force induced by the current, and therefore, the average direction should gradually move to the driving force direction. Eventually, as the current density increases to a threshold value, the moving direction of individual skyrmions will be fully aligned with the force direction. In this saturated case, the pinning force and scattering become a perturbation in comparison with the large driving force.

However, during the elongation of skyrmion through the motion of a half-skyrmion driven by a current, more spins will be flipped along the direction of the effective driving force, which changes the internal structure and energy of this skyrmion, although the skyrmion number is constant. Because the motion of the half-skyrmion is a consequence of the spin flipping caused by current force, only the spins in the direction of the effective driving force can be flipped. The spins away from the effective driving force direction cannot flip because there is not enough energy (or torque) to de-pin the domain walls. Therefore, it is difficult for the half-skyrmion to move away from the driving force direction. Half-skyrmions have three advantages with respect to skyrmions: (i) The Hall angle of the half-skyrmions is independent of the applied current density. (ii) No external field is required for the stabilization of half-skyrmions. (iii) The trajectories of the half-skyrmions could be perfectly recorded/reflected by the elongation of the very narrow strip domains. On the basis of these, we could easily reconstruct the current distributions from the Kerr microscopy image of strip domains.

By tuning the Co thickness, the Hall angles of half-skyrmions can be reduced to as small as 4°. The Hall angle is so small that paths of half-skyrmions approximately delineate the invisible current flow, which have been demonstrated in both the continuous film and the curved track sample.

## MATERIALS AND METHODS

PMA multilayer stacks Ta (5 nm)/Pt (3 nm)/Co (*t*)/Ta (2 nm), with *t* ranging from 1.5 to 2.0 nm, were deposited on thermally oxidized Si substrates, using dc magnetron sputtering (Singulus) at room temperature. The pressure of the Ar gas was set to 0.4 Pa, with a base pressure lower than  $\sim 2 \times 10^{-5}$  Pa. The patterned straight and curved tracks were prepared using lithography and Ar ion milling. Differential polar MOKE measurements were performed using a commercial MOKE microscope from Evico Magnetics. The evolution of the domain structures was imaged and recorded using a quasi-static technique, in which each image was taken in a zero field after each pulse. Note that the domain size and morphology remained almost unchanged at zero external field during the imaging. Voltage pulses were applied with an Agilent arbitrary waveform generator and amplified using a KEPCO bipolar operational power supply/amplifier. Before imaging the paths of the half-skyrmions induced by the current in the track, we applied magnetic field pulses with magnitudes slightly larger than the coercive field and durations of 0.1 s, one by one manually, until the reversed labyrinth-like domain patterns generated in the upward saturated film by the pulses move inside the imaging area. Finite element modeling calculations of electric current distributions were performed using COMSOL Multiphysics. A metallic Co film with a conductivity of  $1.6 \times 10^7$  S m<sup>-1</sup> was chosen as the sample. The size of electrodes and the distance between two electrodes used in the simulations are the same as the experimental configuration.

## SUPPLEMENTARY MATERIALS

Supplementary material for this article is available at <http://advances.sciencemag.org/cgi/content/full/6/6/eaay1876/DC1>

Section S1. Evolution of the domain structure induced by field pulses

Section S2. Theoretical analysis of the half-skyrmion Hall effect

Fig. S1. Hysteresis loops of the samples.

Fig. S2. Evolution of the domain structure induced by field pulses.

Fig. S3. Asymmetric expansion of labyrinth domain.

Fig. S4. Evolution of the domain structure induced by field pulses in films with strong PMA.

Fig. S5. Evolution of the domain structure induced by increased field pulses.

Fig. S6. Hall effect of magnetic half-skyrmion.

Fig. S7. The elongation of a strip domain in the *t* = 1.8 nm film.

Fig. S8. Dependence of  $K_{\text{eff}}$  and domain width on  $\mu_0 H_k$ .

Movie S1. Elongation of a strip domain in the *t* = 1.7 nm film.

Movie S2. Elongation of a strip domain in the *t* = 1.5 nm film.

Movie S3. Current-induced half-skyrmion motion in a curved conduction path.

Reference (39)

## REFERENCES AND NOTES

1. J. R. Kirtley, J. P. Wikswo Jr., Scanning SQUID microscopy. *Annu. Rev. Mater. Sci.* **29**, 117–148 (1999).
2. L. A. Knauss, A. B. Cawthorne, N. Lettsome, S. Kelly, S. Chatrathorn, E. F. Fleet, F. C. Wellstood, W. E. Vanderlinde, Scanning SQUID microscopy for current imaging. *Microelectron. Reliab.* **41**, 1211–1229 (2001).
3. K. Koyanagi, T. Kiss, M. Inoue, T. Nakamura, K. Imamura, M. Takeo, Y. Shiohara, Measurement of local current flow around transverse defects in YBCO film by use of scanning SQUID microscope. *Phys. C Supercond.* **445–448**, 677–681 (2006).
4. J.-P. Tetienne, N. Dontschuk, D. A. Broadway, A. Stacey, D. A. Simpson, L. C. L. Hollenberg, Quantum imaging of current flow in graphene. *Sci. Adv.* **3**, e1602429 (2017).

5. K. C. Nowack, E. M. Spanton, M. Baenninger, M. König, J. R. Kirtley, B. Kalisky, C. Ames, P. Leubner, C. Brüne, H. Buhmann, Imaging currents in HgTe quantum wells in the quantum spin Hall regime. *Nat. Mater.* **12**, 787–791 (2013).
6. Y. Shibata, S. Nomura, H. Kashiwaya, S. Kashiwaya, R. Ishiguro, H. Takayanagi, Imaging of current density distributions with a Nb weak-link scanning nano-SQUID microscope. *Sci. Rep.* **5**, 15097 (2015).
7. M. Inoue, K. Abiru, Y. Honda, T. Kiss, Y. Iijima, K. Kakimoto, T. Saitoh, K. Nakao, Y. Shiohara, Observation of current distribution in high- $T_c$  superconducting tape using scanning Hall-probe microscope. *IEEE Trans. Appl. Supercond.* **19**, 2847–2850 (2009).
8. W. Xing, B. Heinrich, H. Zhou, A. A. Fife, A. Cragg, Magnetic flux mapping, magnetization, and current distributions of  $\text{YBa}_2\text{Cu}_3\text{O}_7$  thin films by scanning Hall probe measurements. *J. Appl. Phys.* **76**, 4244–4255 (1994).
9. S. Yamamoto, S. Schultz, Scanning magnetoresistance microscopy (SMRM): Imaging with a MR head. *J. Appl. Phys.* **81**, 4696–4698 (1997).
10. B. D. Schrag, G. Xiao, Submicron electrical current density imaging of embedded microstructures. *Appl. Phys. Lett.* **82**, 3272–3274 (2003).
11. P. C. Miranda, M. Lomarev, M. Hallett, Modeling the current distribution during transcranial direct current stimulation. *Clin. Neurophysiol.* **117**, 1623–1629 (2006).
12. S. F. Zhang, W. L. Gan, J. Kwon, F. L. Luo, G. J. Lim, J. Wang, W. S. Lew, Highly efficient domain walls injection in perpendicular magnetic anisotropy nanowire. *Sci. Rep.* **6**, 24804 (2016).
13. Y. Hirata, D.-H. Kim, S. K. Kim, D.-K. Lee, S.-H. Oh, D.-Y. Kim, T. Nishimura, T. Okuno, Y. Futakawa, H. Yoshikawa, A. Tsukamoto, Y. Tserkovnyak, Y. Shiota, T. Moriyama, S.-B. Choe, K.-J. Lee, T. Ono, Vanishing skyrmion Hall effect at the angular momentum compensation temperature of a ferrimagnet. *Nat. Nanotechnology* **14**, 232–236 (2019).
14. S. Parkin, S.-H. Yang, Memory on the racetrack. *Nat. Nanotechnol.* **10**, 195–198 (2015).
15. I. M. Miron, K. Garello, G. Gaudin, P.-J. Zermatten, M. V. Costache, S. Auffret, S. Bandiera, B. Rodmacq, A. Schuhl, P. Gambardella, Perpendicular switching of a single ferromagnetic layer induced by in-plane current injection. *Nature* **476**, 189–193 (2011).
16. L. Liu, C.-F. Pai, Y. Li, H. Tseng, D. Ralph, R. Buhrman, Spin-torque switching with the giant spin Hall effect of tantalum. *Science* **336**, 555–558 (2012).
17. L. Liu, O. Lee, T. J. Gudmundsen, D. C. Ralph, R. A. Buhrman, Current-induced switching of perpendicularly magnetized magnetic layers using spin torque from the spin Hall effect. *Phys. Rev. Lett.* **109**, 096602 (2012).
18. B. Jinnai, C. Zhang, A. Kurenkov, M. Bersweiller, H. Sato, S. Fukami, H. Ohno, Spin-orbit torque induced magnetization switching in Co/Pt multilayers. *Appl. Phys. Lett.* **111**, 102402 (2017).
19. P. P. Haazen, E. Murè, J. H. Franken, R. Lavrijsen, H. J. M. Swagten, B. Koopmans, Domain wall depinning governed by the spin Hall effect. *Nat. Mater.* **12**, 299–303 (2013).
20. S. Fukami, T. Anekawa, C. Zhang, H. Ohno, A spin-orbit torque switching scheme with collinear magnetic easy axis and current configuration. *Nat. Nanotechnol.* **11**, 621–625 (2016).
21. S. Woo, K. Litzius, B. Krüger, M.-Y. Im, L. Caretta, K. Richter, M. Mann, A. Krone, R. M. Reeve, M. Weigand, P. Agrawal, I. Lemesch, M.-A. Mawass, P. Fischer, M. Kläui, G. S. D. Beach, Observation of room-temperature magnetic skyrmions and their current-driven dynamics in ultrathin metallic ferromagnets. *Nat. Mater.* **15**, 501–506 (2016).
22. W. Jiang, X. Zhang, G. Yu, W. Zhang, X. Wang, M. B. Jungfleisch, J. E. Pearson, X. Cheng, O. Heinonen, K. L. Wang, Y. Zhou, A. Hoffmann, S. G. E. te Velthuis, Direct observation of the skyrmion Hall effect. *Nat. Phys.* **13**, 162–169 (2017).
23. K. Litzius, I. Lemesch, B. Krüger, P. Bassirian, L. Caretta, K. Richter, F. Büttner, K. Sato, O. A. Tretiakov, J. Förster, R. M. Reeve, M. Weigand, I. Bykova, H. Stoll, G. Schütz, G. S. D. Beach, M. Kläui, Skyrmion Hall effect revealed by direct time-resolved x-ray microscopy. *Nat. Phys.* **13**, 170–175 (2016).
24. A. Salimath, A. Abbott, A. Brataas, A. Manchon, Current-driven skyrmion depinning in magnetic granular films. *Phys. Rev. B* **99**, 104416 (2019).
25. W. Jiang, P. Upadhyaya, W. Zhang, G. Yu, M. B. Jungfleisch, F. Y. Fradin, J. E. Pearson, Y. Tserkovnyak, K. L. Wang, O. Heinonen, S. G. E. te Velthuis, A. Hoffmann, Blowing magnetic skyrmion bubbles. *Science* **349**, 283–286 (2015).
26. C. Moreau-Lucaire, C. Moutafis, N. Reyren, J. Sampaio, C. A. F. Vaz, N. Van Horne, K. Bouzehouane, K. Garcia, C. Deranlot, P. Warnicke, P. Wohlhüter, J.-M. George, M. Weigand, J. Raabe, V. Cros, A. Fert, Additive interfacial chiral interaction in multilayers for stabilization of small individual skyrmions at room temperature. *Nat. Nanotechnol.* **11**, 444–448 (2016).
27. G. Yu, P. Upadhyaya, Q. Shao, H. Wu, G. Yin, X. Li, C. He, W. Jiang, X. Han, P. K. Amiri, K. L. Wang, Room-temperature skyrmion shift device for memory application. *Nano Lett.* **17**, 261–268 (2017).
28. A. Fert, N. Reyren, V. Cros, Magnetic skyrmions: Advances in physics and potential applications. *Nat. Rev. Mater.* **2**, 17031 (2017).
29. W. Legrand, D. Maccariello, N. Reyren, K. Garcia, C. Moutafis, C. Moreau-Lucaire, S. Collin, K. Bouzehouane, V. Cros, A. Fert, Room-temperature current-induced generation and motion of sub-100 nm skyrmions. *Nano Lett.* **17**, 2703–2712 (2017).
30. S. Zhang, J. Zhang, Y. Wen, E. M. Chudnovsky, X. Zhang, Determination of chirality and density control of Néel-type skyrmions with in-plane magnetic field. *Commun. Phys.* **1**, 36 (2018).
31. S. Zhang, J. Zhang, Y. Wen, E. M. Chudnovsky, X. Zhang, Creation of a thermally assisted skyrmion lattice in Pt/Co/Ta multilayer films. *Appl. Phys. Lett.* **113**, 192403 (2018).
32. Y. Zhou, Magnetic skyrmions: Intriguing physics and new spintronic device concepts. *Natl. Sci. Rev.* **6**, 210–212 (2018).
33. G. Yu, P. Upadhyaya, X. Li, W. Li, S. K. Kim, Y. Fan, K. L. Wong, Y. Tserkovnyak, P. K. Amiri, K. L. Wang, Room-temperature creation and spin-orbit torque manipulation of skyrmions in thin films with engineered asymmetry. *Nano Lett.* **16**, 1981–1988 (2016).
34. M. He, G. Li, Z. Zhu, Y. Zhang, L. Peng, R. Li, J. Li, H. Wei, T. Zhao, X.-G. Zhang, S. Wang, S.-Z. Lin, L. Gu, G. Yu, J. W. Cai, B.-g. Shen, Evolution of topological skyrmions across the spin reorientation transition in Pt/Co/Ta multilayers. *Phys. Rev. B* **97**, 174419 (2018).
35. A. A. Thiele, Steady-state motion of magnetic domains. *Phys. Rev. Lett.* **30**, 230–233 (1973).
36. P. J. Metaxas, J. P. Jamet, A. Mougin, M. Cormier, J. Ferré, V. Baltz, B. Rodmacq, B. Dieny, R. L. Stamps, Creep and flow regimes of magnetic domain-wall motion in ultrathin Pt/Co/Pt films with perpendicular anisotropy. *Phys. Rev. Lett.* **99**, 217208 (2007).
37. J. Sampaio, V. Cros, S. Rohart, A. Thiaville, A. Fert, Nucleation, stability and current-induced motion of isolated magnetic skyrmions in nanostructures. *Nat. Nanotechnol.* **8**, 839–844 (2013).
38. S. Zhang, J. Wang, Q. Zheng, Q. Zhu, X. Liu, S. Chen, C. Jin, Q. Liu, C. Jia, D. Xue, Current-induced magnetic skyrmions oscillator. *New J. Phys.* **17**, 023061 (2015).
39. A. Hrabec, N. A. Porter, A. Wells, M. J. Benitez, G. Burnell, S. McVitie, D. McGrouther, T. A. Moore, C. H. Marrows, Measuring and tailoring the Dzyaloshinskii-Moriya interaction in perpendicularly magnetized thin films. *Phys. Rev. B* **90**, 020402 (2014).

#### Acknowledgments

**Funding:** This publication is based on research supported by the King Abdullah University of Science and Technology (KAUST), Office of Sponsored Research (OSR), under award nos. OSR-2016-CRG5-2977, OSR-2017-CRG6-3427, and CRF-2015-SENSORS-2708. X.Z. acknowledges the support by the Presidential Postdoctoral Fellowship of The Chinese University of Hong Kong, Shenzhen (CUHKSZ). Y.Z. acknowledges the support by the President's Fund of CUHKSZ, Longgang Key Laboratory of Applied Spintronics, National Natural Science Foundation of China (grant no. 11574137) and Shenzhen Fundamental Research Fund (grant nos. JCYJ20160331164412545 and JCYJ20170410171958839). W.W. acknowledge financial support by the National Key R&D Program of China (no. 2017YFA0303202). **Author contributions:** S.Z. and X.-X.Z. conceived and coordinated the project and analyzed the data. X.Z., J.X., and Y.Z. developed the theoretical model. Y.W. and S.Z. fabricated the samples, and S.Z. performed the MOKE measurements. S.Z., X.Z., and X.-X.Z. wrote the manuscript. The study was supervised by X.-X.Z. All authors contributed to the discussion and preparation of the manuscript. **Competing interests:** The authors declare that they have no competing interests. **Data and materials availability:** All data needed to evaluate the conclusions in the paper are present in the paper and/or the Supplementary Materials. Additional data related to this paper may be requested from the authors.

Submitted 28 May 2019

Accepted 22 November 2019

Published 7 February 2020

10.1126/sciadv.aay1876

**Citation:** S. Zhang, X. Zhang, J. Zhang, A. Ganguly, J. Xia, Y. Wen, Q. Zhang, G. Yu, Z. Hou, W. Wang, Y. Peng, G. Xiao, A. Manchon, J. Kosel, Y. Zhou, X.-X. Zhang, Direct imaging of an inhomogeneous electric current distribution using the trajectory of magnetic half-skyrmions. *Sci. Adv.* **6**, eaay1876 (2020).

## Direct imaging of an inhomogeneous electric current distribution using the trajectory of magnetic half-skyrmions

Senfu Zhang, Xichao Zhang, Junwei Zhang, Arnab Ganguly, Jing Xia, Yan Wen, Qiang Zhang, Guoqiang Yu, Zhipeng Hou, Wenhong Wang, Yong Peng, Gang Xiao, Aurelien Manchon, Jrgen Kosel, Yan Zhou, and Xi-Xiang Zhang

*Sci. Adv.*, **6** (6), eaay1876.

DOI: 10.1126/sciadv.aay1876

### View the article online

<https://www.science.org/doi/10.1126/sciadv.aay1876>

### Permissions

<https://www.science.org/help/reprints-and-permissions>

Use of this article is subject to the [Terms of service](#)

---

*Science Advances* (ISSN 2375-2548) is published by the American Association for the Advancement of Science. 1200 New York Avenue NW, Washington, DC 20005. The title *Science Advances* is a registered trademark of AAAS.

Copyright © 2020 The Authors, some rights reserved; exclusive licensee American Association for the Advancement of Science. No claim to original U.S. Government Works. Distributed under a Creative Commons Attribution NonCommercial License 4.0 (CC BY-NC).